Polymer 49 (2008) 2223–2234

Contents lists available at ScienceDirect

Polymer

journal homepage: www.elsevier.com/locate/polymer

Evaluation of nanoparticulate fillers for development of shape memory polyurethane nanocomposites

I. Sedat Gunes, Feina Cao, Sadhan C. Jana *

Department of Polymer Engineering, The University of Akron, Akron, OH 44325-0301, United States

ARTICLE INFO

Article history:
Received 16 January 2008
Received in revised form 5 March 2008
Accepted 13 March 2008
Available online 16 March 2008

Keywords:
Shape memory polymer
Nanocomposite
Polyurethanes

ABSTRACT

The effects of nano-size fillers on shape memory (SM) properties of polyurethane (PU) nanocomposites were evaluated. Organoclay, carbon nanofiber (CNF), silicon carbide (SiC), and carbon black (CB) were selected as the fillers in an attempt to reinforce the PU and to obtain significantly increased shape recovery stress. The shape memory PU was synthesized from diphenylmethane diisocyanate, 1,4-butanediol, and poly(caprolactone)diol, the latter with a molecular weight of 4000 g/mol. The composites were prepared by melt mixing of extended chain PU with the fillers. The shape memory behavior was triggered by heating the specimen above the melting point of the crystalline soft segment. Our results indicate that exfoliated organoclay significantly augments SM performance, while CNF and SiC diminish it by interfering with crystallization of the soft segment. CB destroys the shape memory properties beyond a certain loading. Better SM performance with organoclay can be attributed to mechanical reinforcement without much interference with the soft segment crystallinity. The reduction of soft segment crystallinity in the presence of CNF and SiC was analyzed. It was found that the extent of crystallinity, as well as the crystallization temperature, was significantly reduced in the presence of these fillers.

1. Introduction

Shape memory polymer (SMP) is a stimuli responsive material, which may recover its original shape from large deformation and extended period of cold hibernation. A basic mechanism of shape recovery can be attributed to 'shrinkage' of oriented, extended chains triggered, for example, by melting or glass transition [1]. SMPs recovering by this mechanism can be defined as *rubberlike* SMP [2]. Other definitions of shape memory polymers can be found elsewhere [3–5]. External stimuli, such as heat [6,7], electric field [8], magnetic field [9], and light [10] have been used to trigger shape changes of SMPs. Note, however, that in all these cases, the external stimuli generated heat, e.g., by Joule heating in electric field [8], induction heating in magnetic field [9], or by photon absorption [10] which in turn led to glass transition or melting of oriented, extended polymer chains.

SMPs are usually multiphase materials comprised of a *fixed* or *hard* phase and a *reversible* or *soft* phase. The *fixed* phase acts in the same manner as thermally stable cross-link points even at elevated temperatures. The 'cross-links' may be of physical or chemical nature, e.g., crystals, glassy domains, chain entanglements, or chemical cross-links that prevent 'free' flow of surrounding polymer chains upon application of stress. The *reversible* phase, on the other hand, is the main constituent and is responsible for elasticity [11,12].

The basic advantages of SMPs over other shape memory (SM) materials, e.g., metals, such as shape memory alloys (SMAs) are its inherently high recoverable strain of several hundred percents [13] and much lower density. In addition, SMPs possess conveniently adjustable material properties and can be easily produced and shaped by conventional polymer processing techniques. Nevertheless, there are some scientific and technological barriers which prevent widespread applications of SMP. For instance, SMPs have relatively low recovery stress, which is usually 1–3 MPa compared to 0.5–1 GPa for shape memory metal alloys [3]. The relatively low recovery stress becomes a limiting factor in many applications especially in cases where SMP articles should overcome a large resisting stress during shape recovery.

Various fillers – nano- or microscopic – have been considered in prior work on shape memory polymer composites in efforts to augment mechanical properties and to derive multiple functionalities. A review of literature on particle filled SMPs can be found in Ref. [2]. It has been observed that there is a trade-off between enhancement of modulus and reduction of recoverable strain ratio. Generally, fillers exert negative impact on recoverable strain due to their size, and substantially higher stiffness compared to the matrix polymer. In some cases, they even disturb the polymer networks responsible for shape memory functions, especially at high loading

* Corresponding author. Tel.: +1 330 972 8293; fax: +1 330 258 2339.
E-mail address: janas@uakron.edu (S.C. Jana).

0032-3861/$ – see front matter © 2008 Elsevier Ltd. All rights reserved.
doi:10.1016/j.polymer.2008.03.021

levels. As will be apparent below, research efforts to strike a balance between the recovery stress and the recovery strain with the use of fillers are still evolving.

PU and its particle filled composites have been a popular choice as SMPs due to their versatility and relative ease of preparation. Pioneering works in the area of shape memory PU (SMPU) date back to several decades. The first patent on PU foam was issued in 1966 [14]. Hayashi [15] and Tobushi and coworkers [16,17] described basic properties of SMPU thin films and foams in a series of articles. Liang et al. [18] and Ohki et al. [19] observed severe deterioration of shape memory performance in SMPU in the presence of chopped and woven fiberglass and unidirectional Kevlar fibers. Li et al. [20] and Yang et al. [21] also reported negative impact of fillers on SM properties in CB/SMPU composites. Gall et al. [22,23] reported enhanced mechanical properties of an epoxy SMP with SiC of average diameters of 0.3–0.7 μm. Mondal and Hu [24] and Koerner et al. [25] observed improved recovery ratio and higher recovery stress of SMPU in the presence of multi-wall carbon nanotubes (MWNTs). Recently, Cao and Jana [26] reported the first organoclay/SMPU nanocomposites with promising SM properties. They observed a 25% increase in shape recovery stress with the use of 1 wt% nanoclay in SMPU based on poly(caprolactone)diol (PCL diol).

In this work, the effects of four filler particles – organoclay, carbon nanofiber (CNF), silicon carbide (SiC), and carbon black (CB) – on shape memory behavior of SMPU were investigated. The SMPU was synthesized with crystalline soft segments from PCL diol, as reported earlier by Cao and Jana [26]. As will be discussed later, true nanocomposites were produced only in the case of organoclay and silicon carbide nanoparticles.

2. Experimental

2.1. Materials

A few words are in order on the selection of monomers for SMPU synthesis. Various common diisocyanates, such as diphenylmethane diisocyanate (MDI), and chain extenders, such as 1,4-butanediol (BD), have been used in the synthesis of SMPU [3]. Selection of polyol type is more critical, since it adds the capability of preserving the deformation-induced segmental orientation of soft segments either by crystallization or by vitrification [2]. PCL diol has been a popular choice [2] due to its relative ease of crystallization [27]. Polyols with relatively long relaxation times, such as poly(tetramethyleneglycol)diol (PTMG diol) [28], have been used in cases where glassy soft segments are desired [2]. In this work, we selected PCL diol as the polyol and prepared an SMPU with a crystalline soft segment due to certain potential advantages over a glassy one. First, the temperature interval required for shape recovery in a crystalline system is usually narrower than that of a glassy one, since crystal melting is a first-order transition whereas glass transition is a second-order one. This in turn provides a relatively sharp and more complete shape recovery over a more definite and narrow temperature range. Second, crystalline soft segments usually contribute higher toughness to the resultant materials which is a critical design parameter in engineering applications.

In this work, SMPU with 33 wt% hard segment content was synthesized using a molar ratio of 6/5/1 of, respectively, MDI (Bayer MaterialScience, Pittsburgh, PA), BD (Avocado Organics, UK), and PCL diol (Solvay Chemical, UK), the latter with a molecular weight of 4000 g/mol. A set of representative physical properties of these monomers are presented in Table 1. A tin catalyst, DABCO T120 (Air Products, Allentown, PA), was used to expedite the chain extension reactions. Cloisite® 30B from Southern Clay Products (Gonzalez, TX) was selected as the organoclay. Cloisite® 30B contained organic quaternary ammonium ions $N^+(CH_2CH_2OH)_2(CH_3)T$, where T represents an alkyl group with approximately 65% $C_{18}H_{37}$, 30% $C_{16}H_{33}$, and 5% $C_{14}H_{29}$. Pyrograph III® CNF was obtained from Applied Sciences, Inc. (Cedarville, OH) in the form of PR-24-PS, a vapor grown and pyrolytically stripped material with fiber diameter of 60–200 nm and length of 30–100 μm. SiC was obtained in β-crystalline form (NanoSiC®) from MTI Corp. (Richmond, CA) with an average size smaller than 30 nm and a density of 3.22 g/cm^3. A high structure, conductive CB grade was obtained from Akzo Nobel (Norcross, GA), grade Ketjenblack® EC 300J. This grade of CB offered a pore volume of 0.310–0.345 $\times 10^{-3}$ m^3/100 g determined by dibutyl phthalate absorption [29].

Table 1
Physical properties of monomers

Monomer	MW (g/mol)	Density (g/cm^3)	Melting point (°C)
MDI	250	1.19	39
PCL diol	4000	1.07	55–60
BD	90	1.01	20

2.2. Sample preparation

All fillers were dried overnight under vacuum at 120 °C to eliminate any absorbed moisture. BD and PCL diol were also dried overnight under vacuum at 45 °C. The prepolymer was synthesized at 80 °C by reacting MDI and PCL diol for 2.5 h, under nitrogen with mechanical stirring. Chain extension of prepolymer was carried out in Brabender Plasticorder (model EPL 7752) at 90 °C by mixing with BD for 25 min in the presence of 2×10^{-7} mol/L of tin catalyst. The molar ratio of isocyanate and alcoholic –OH groups in the composite was maintained at 1:1 and the amount of BD in chain extension step was adjusted accordingly by taking into account the $-CH_2CH_2OH$ groups in the quaternary ammonium ions in Cloisite® 30B clay [26,30–35]. Organoclay/SMPU nanocomposite was prepared by adding the desired amounts of clay to the reaction mixture after 5 min of chain extension reaction and further mixing for 20 min. A detailed account of the method used for the preparation of organoclay/SMPU nanocomposite is presented elsewhere [26,30–32]. The temperature rose to 150 °C upon the addition of clay particles and then stabilized at 145 °C. This mixing and reaction scheme allowed formation of exfoliated nanocomposites [26,30–32]. In the composites of CNF, SiC, and CB, a stoichiometric amount of BD was used in the chain extension step. The chain extension was fully carried out at 110 °C for 2 min before addition of the filler particles. The filler particles were mixed with the polymer for another 5 min with a set temperature of 140 °C, although the temperature rose to 165 °C with the addition of filler particles and then stabilized at 160 °C. The total filler content was maintained between 1 wt% and 5 wt%. The composites were compression molded in an electrically heated compression molder to produce specimens with a thickness of 0.5 mm for further testing. The set temperature of compression molder platens was 220 °C, shot size was kept at about 60 g, and compression pressure was 25 MPa. The compression molding cycle time was kept at about 3 min to prevent any thermal degradation. The molded samples were further cold compressed at room temperature in another compression molder for 15 min under a pressure of 25 MPa.

2.3. Testing and characterization

The state of organoclay dispersion was evaluated from wide-angle X-ray diffraction (WAXD) patterns. For this purpose, an X-ray diffractometer (Rigaku, Japan) with wavelength $\lambda = 0.154$ nm, a tube voltage of 40 kV, and tube current of 150 mA was used. A scanning range of $2\theta = 1.5$–10° was used with a scanning interval of 0.05°. The specimens with thickness of about 70 nm were microtomed under cryogenic conditions using Reichert Ultracut S/FC S

ultramicrotome (Leica, Germany) to obtain transmission electron microscopic (TEM) images with JEOL TEM device (JEM-1200EXII) at 120 kV. The scanning electron microscopic (SEM) images were obtained by sputter coating the cryogenically fractured surfaces with silver using a K575x sputter coater (Emitech, UK) under argon atmosphere. The SEM images were generated with a SEM S-2150 microscope (Hitachi, Japan) at 20 kV.

Tensile tests (ASTM D882) were performed at room temperature and at 60 °C using Instron 4204 (Norwood, MA), equipped with a heating chamber. The tests were conducted at a crosshead speed of 50 mm/min. The hysteresis in stress–strain relationship was determined using a set of samples stretched only once (designated as Cycle I) and a second set of samples stretched for the second time after the initial shape recovery process (designated as Cycle II). For each condition, three different specimens were tested and the arithmetic average of properties was noted. The repeatability of experiments was observed to be high, with a standard deviation of about 10%.

In order to evaluate the shape memory properties, the specimens were stretched at 60 °C at a strain rate of 50 mm/min to predefined stretching ratios of 30%, 60%, and 100%. The specimens were then cooled quickly down to room temperature with the aid of a fan. A few words are in order on the cooling behavior of the composites. It was reported earlier that cooling of specimens by fan resulted in relatively high cooling rates [26]. In the context of present study, one may argue, however, the potential differences in heat transfer rates due to potentially different thermal transport properties of the filler particles. We found that all composites cooled in similar fashion aided by fairly small specimen thicknesses of about 0.5 mm and relatively high cooling rates due to strong forced convection. Besides, maximum filler loadings of about 2–3 vol% were used in this work. These small filler loadings should not exert any appreciable impact on the thermal conductivity of composites, as found by other investigators [36–39].

Let us now describe a typical shape memory testing cycle shown in Fig. 1. In this figure, l_o is the original length of the sample at room temperature (T_{cold}), l_s is the length after stretching at temperature T_{hot} (~60 °C) with tensile load in place, l_D is the sample length just after release of the tensile load, and l_f is the final recovered length of the stretched sample after going through shape recovery. The performance parameters related to SM testing are defined as follows. Shape fixity (SF) is defined as the level of deformation that may be fixed upon rapid cooling of the deformed materials to room temperature in stage B (Fig. 1). The value of SF is computed from the parameters defined in Fig. 1 as follows:

$$SF = \frac{l_D - l_o}{l_s - l_o} \quad (1)$$

The recovery ratio (RR) is the level of deformation that is recovered upon heating in stage C (Fig. 1) and is defined as:

$$RR = \frac{l_D - l_f}{l_D - l_o} \quad (2)$$

For an ideal SMP, the values of SF and RR are 100% indicating that l_s equals to l_D, and l_o equals to l_f. A typical shape recovery test was conducted using a specimen cut from the middle section of the stretched samples. RR was determined from Eq. (2) after heating the specimen in stationary hot water at 60 °C. The recovery in hot water is instantaneous and specimen recovered as soon as it contacted hot water due to high rate of conductive heat transfer and low specimen thicknesses. The recovery in hot water represents unconstrained recovery of the shape. A Perkin–Elmer Pyris Diamond dynamic mechanical analyzer (DMA) (Waltham, MA) operating in L-control mode was used to determine the recovery stress which was the peak value of the stress during heating. A typical rectangular specimen of 20 mm in length, 2 mm in width, and 0.5 mm in thickness was fixed at room temperature between the clamps of DMA set up and heated at a rate of 10 °C/min to approximately 80 °C.

The thermal properties, such as melting point and crystallinity of the soft segment, were determined using a differential scanning calorimetric device (TA instruments DSC-29210, New Castle, DE) under nitrogen atmosphere. During the first thermal scan, the specimens were heated at a scanning rate of 10 °C/min to 250 °C and then quenched to −100 °C at an average cooling rate of 70 °C/min using liquid nitrogen. The specimen was subjected to second thermal scan over a temperature range of −100 °C to 250 °C with a heating rate of 10 °C/min. The first thermal scan was relatively more representative of the actual SM testing cycle. The second thermal scan with cooling down to −100 °C was performed to gain further insight on crystallization behavior of the composites in the presence of various fillers. In cooling experiments, the specimen was heated to 70 °C, kept at this temperature for 5 min, and cooled down to −50 °C with cooling rates of 10 °C/min and 20 °C/min.

The nature of surface functional groups on SiC particles was determined using X-ray photoelectron spectroscopic (XPS) method. The XPS spectra were obtained using a Kratos Model ES3000 spectrometer (Manchester, UK) under high vacuum conditions with a pressure of 10^{-8} Torr, an aluminum anode, and a resolution of 1 eV. The assignment of peak locations and corresponding fitting of XPS spectra were performed with a curve fitting and data analysis software Fityk 0.7.7 (http://www.unipress.waw.pl/fityk).

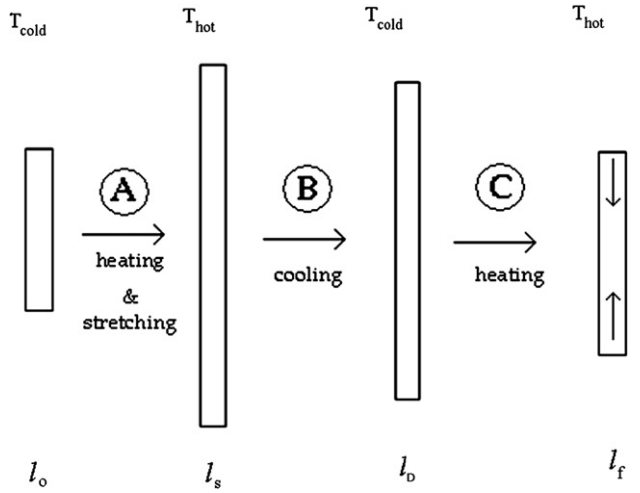

Fig. 1. Schematic describing stages of sample deformation by tensile stress in a typical SM testing cycle. The specimen attained a temperature of 60 °C before it was stretched at 50 mm/min in stage A. The specimen was cooled from 60 °C to room temperature using a cooling fan (stage B). The specimen was heated from room temperature at a rate of 10 °C/min to obtain shape recovery in stage C.

3. Results and discussion

3.1. Filler dispersion in composites

Both TEM images and WAXD patterns of organoclay nanocomposites indicated well exfoliated organoclay platelets. A set of representative TEM images is presented in Fig. 2. The composite with 5 wt% clay showed a very small peak at $2\theta = 6.5°$, and a shoulder at $2\theta = 3.4°$ in WAXD (not shown). The corresponding TEM image in Fig. 2(c) showed single platelets and tactoids with an average of 3–4 platelets per tactoid. The TEM images presented in Fig. 2 indicated well dispersed organoclay platelets in SMPU.

The level of dispersion of CNF in SMPU was inferred from SEM of cold fractured surfaces. The SEM image of the composite of 5 wt%

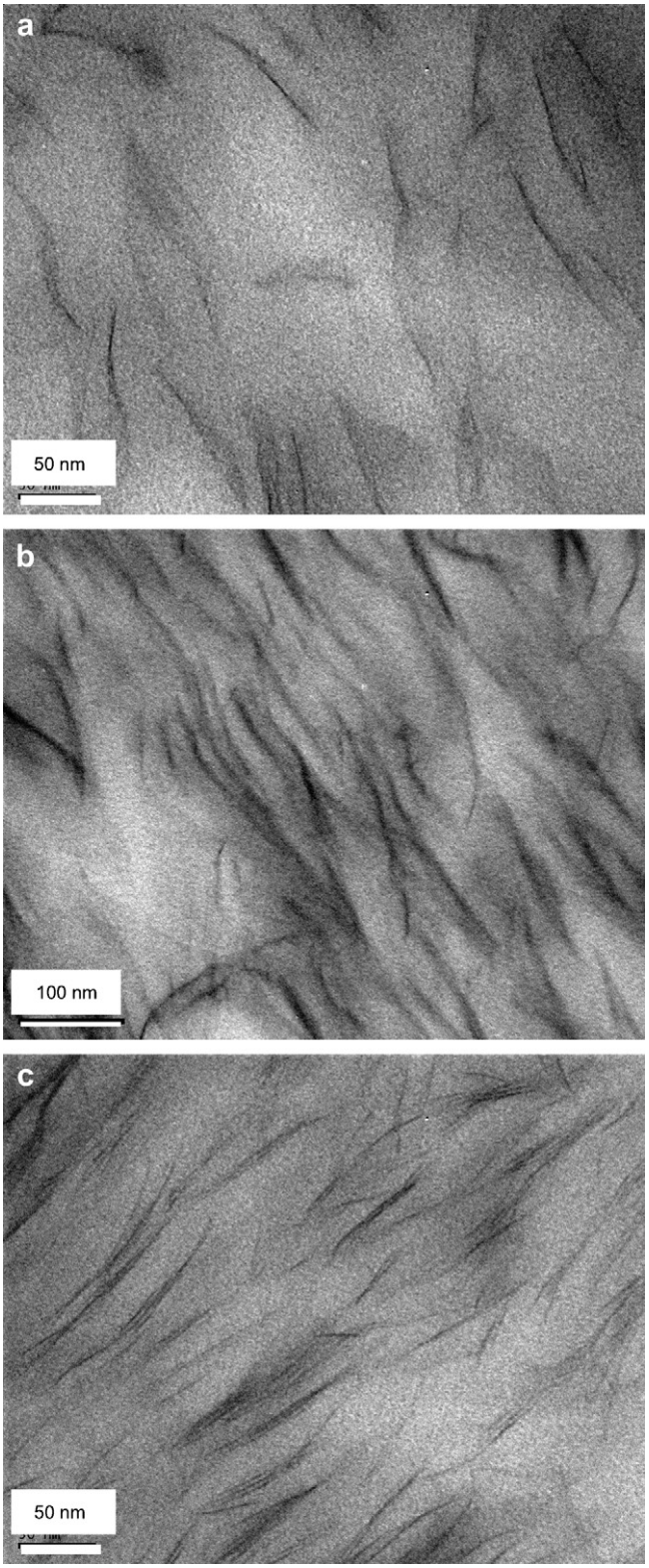

Fig. 2. TEM images of organoclay/SMPU nanocomposites: (a) 1 wt% nanoclay (b) 3 wt% nanoclay (c) 5 wt% nanoclay.

CNF presented in Fig. 3 suggests incomplete dispersion of CNF in the matrix, as fiber bundles can be identified (circled portion in Fig. 3). Similar observations were made earlier by Jimenez and Jana [40,41].

The level of dispersion of SiC particles in SiC/SMPU composites can be inferred from Fig. 4. The TEM image (Fig. 4a) shows that

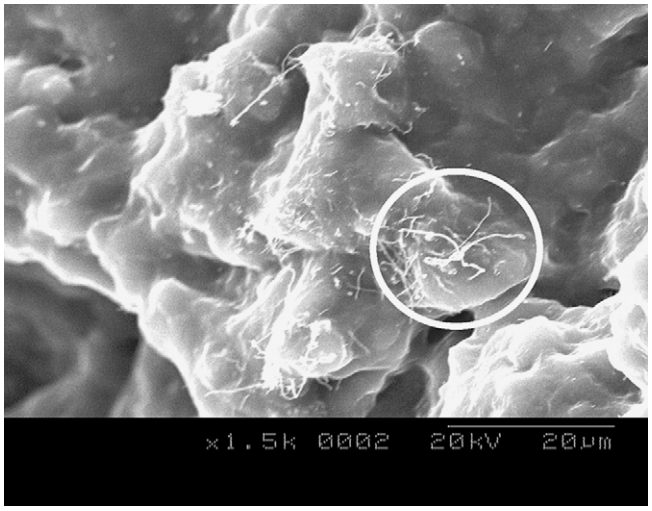

Fig. 3. SEM image of CNF/SMPU composite with 5 wt% filler.

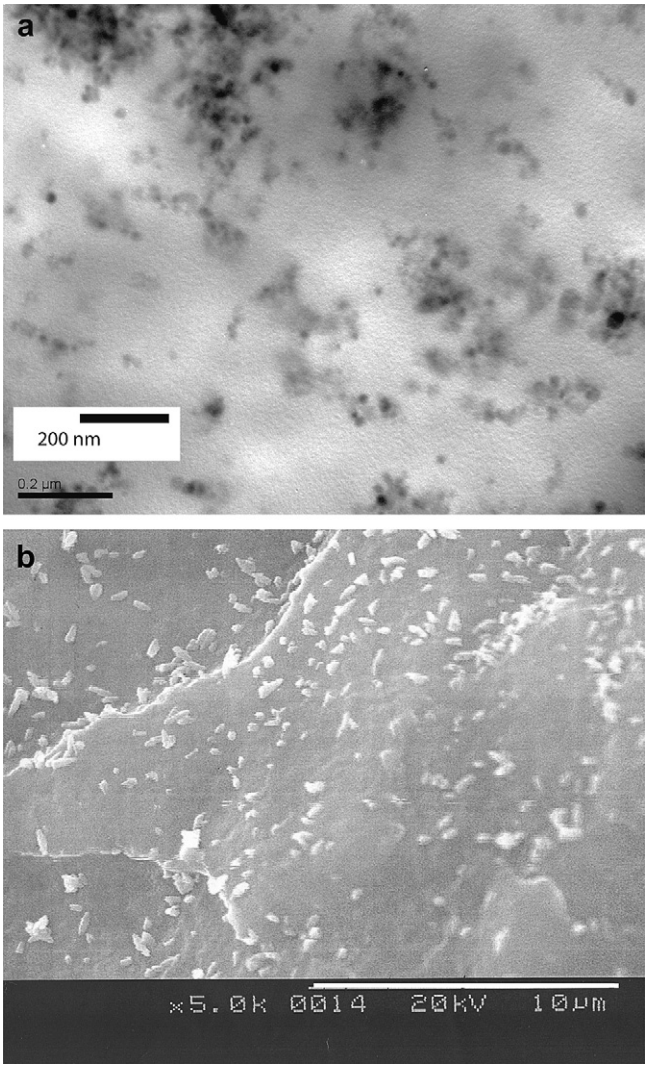

Fig. 4. TEM and SEM images of SiC/SMPU composites with 5 wt% filler. (a) TEM image at high magnification indicating coexistence of filler agglomerates and individually dispersed SiC particles. (b) SEM image at low magnification indicating good overall dispersion of SiC particle agglomerates.

some filler particles dispersed to the scale of single particles. In addition, some particle agglomerates with an average size of about 300–400 nm are seen in SEM image (Fig. 4b), similar to earlier reports [42,43]. Fig. 4b also reveals that SiC particle agglomerates were very well dispersed. In the following section, we will analyze XPS data to learn that such good dispersion of SiC was achieved due to oxygen containing polar functional groups on the surface of SiC particles.

3.2. XPS analysis

The full XPS spectrum of SiC is presented in Fig. 5. It is seen from a strong peak centered at around 533 eV due to O1s that SiC particles contained substantial quantities of oxygen on the surface. The XPS spectrum shown in Fig. 5 was analyzed and it was found that the surface of SiC particles contained 60.8% carbon, 11.3% oxygen, and 27.9% silicon. The C1s and Si2p peaks in XPS spectrum were analyzed further. From Fig. 6 it is revealed that the C1s peak can be deconvoluted into five peaks which were assigned as follows. The peak at around 282.6 eV (peak I) was due to SiC [44], and the peak at around 284.5 eV (peak II) was due to groups containing C–C or C–H bonds [45]. The remaining two peaks at 285.5 eV (peak III) and 283.4 eV (peak IV) were assigned to siliconoxycarbides [46]. The fifth peak at 288.8 eV (peak V) was assigned to O–C=O groups [47], an example of which is COOH [48]. The data for Si2p region also support these assignments, for example, SiC peak was at 99.6 eV [44], silica at 102.4 eV [44], and three peaks for siliconoxycarbides at 100.1 eV, 100.6 eV, and 101.3 eV [44]. It is known that oxygen containing polar functional groups on SiC particle surface originate from surface oxidation of SiC at room temperature [49], although bulk SiC shows significant stability towards oxidation [50,51]. In this study, the oxygen containing polar groups aided dispersion of SiC particles in SMPU, as already shown in Fig. 4. As will be discussed in the next sections, the well dispersed SiC particles exerted detrimental effects on the shape memory properties of SMPU.

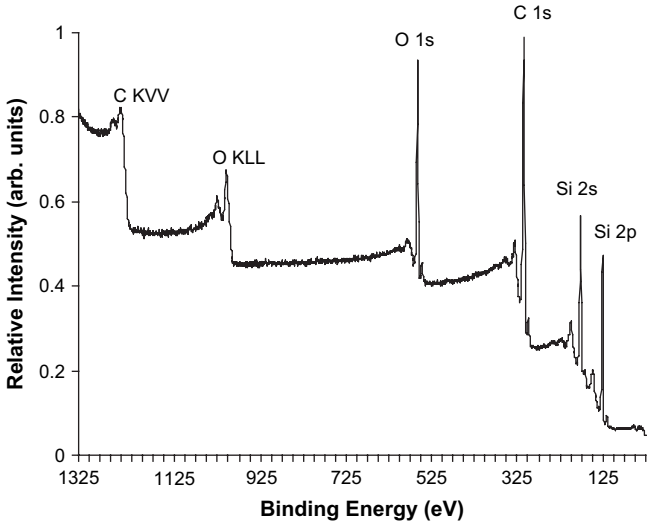

Fig. 5. XPS spectrum of SiC.

3.3. Soft segment crystallinity

It is observed from Fig. 7 that soft segment crystallinity in pristine SMPU was approximately 28% as measured from the first thermal scan in DSC. Recall that the first thermal scan was relatively more representative of the actual SM testing cycle as compared to the second thermal scan. In the calculations of crystallinity, the heat of fusion of fully crystalline PCL was taken to be 32.4 cal/g [52]. The

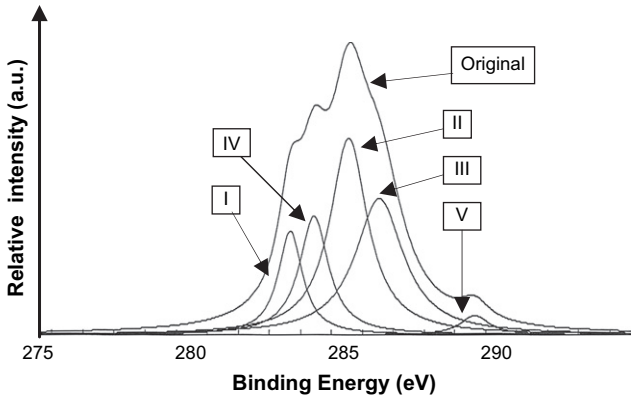

Fig. 6. The C1s region of XPS of SiC resolved into five peaks.

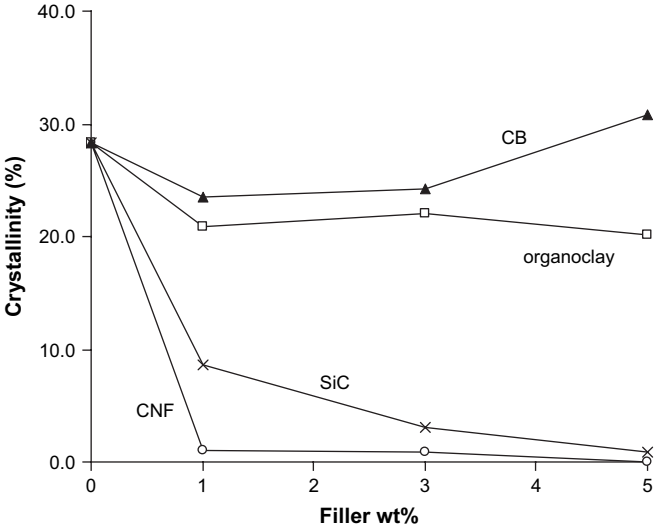

Fig. 7. Soft segment crystallinity of composites after first thermal scan.

crystallinity of neat PCL diol was also determined under the same heating and cooling conditions as experienced by SMPU specimens. It was found that the crystallinity of PCL diol was approximately 65% in the first scan and 59% in the second scan (Table 2). These values are comparable to about 60% as reported in the literature [27,53]. The crystallinity of PCL diol soft segments, however, reduced after incorporation in the PU chains, as was observed by other investigators [27,54]. This can be attributed to the hard segments in PU hindering the mobility of PCL diol soft segments, and preventing close packing of the PCL diol chain segments. We also observed that all materials including neat SMPU and the composites underwent strain induced crystallization during stretching as reported earlier [26,55–58]. Thus, the increase in all shape memory properties at higher stretching ratios is a consequence of strain induced crystallization. Note that the crystals acted as a means to

Table 2
Crystallinity of PCL diol composites

	Crystallinity (%)	
	First scan	Second scan
Neat PCL diol	65	59
Organoclay/PCL diol	56	56
CB/PCL diol	58	52
CNF/PCL diol	59	56
SiC/PCL diol	54	48

Filler content was kept at 10 wt%.

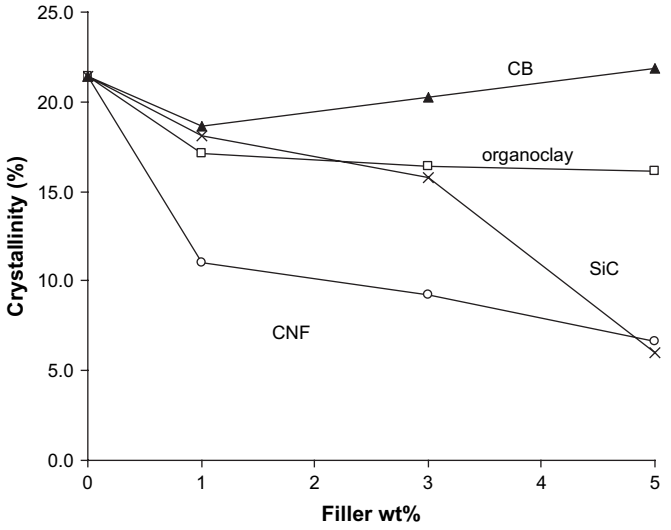

Fig. 8. Soft segment crystallinity of composites after second thermal scan.

keep the chains oriented upon removal of the tensile load in our system (Fig. 1).

The influence of fillers on soft segment crystallinity was determined by DSC. These data are presented in Figs. 7 and 8 as a function of filler content. Note that due to different densities of fillers (1.95 g/cm^3 for CNF [40], 2.83 g/cm^3 for organoclay [59], 3.22 g/cm^3 for SiC [60], and 1.8 g/cm^3 for CB [61]), the maximum volumetric filler content in composites varied between 2% and 3%. The data presented in Fig. 7 represent soft segment crystallinity of unstretched samples after the first thermal scan. The data shown in Fig. 8 were obtained from the second thermal scan. Note that the materials were cooled to −100 °C in the second scan and, therefore, these data indicate the effect of supercooling on crystallinity. The crystallinity of composites of CNF and SiC after the first scan (Fig. 7) shows an enormous decrease as compared to pristine SMPU. In contrast, only marginal changes were observed in the case of organoclay and CB. The same trend is also evident in Fig. 8. It is also evident from Fig. 8 that supercooling down to −100 °C increased the level of soft segment crystallinity to relatively higher values, as compared to results presented in Fig. 7. The peak temperatures for crystal melting are presented in Table 3. It is observed that the presence of organoclay and CB did not significantly reduce the melting point. However, the melting points of soft segment crystals were remarkably reduced in the presence of CNF and SiC. It is known that the melting point is dictated by the crystal size [62], hence it can be inferred that CNF or SiC addition decreased the overall crystallinity and possibly the crystal size.

To gain more insight on the effects of fillers on crystallization of PCL diol soft segments, a series of crystallization experiments were performed in DSC, in addition to the crystal melting experiments mentioned above. Representative DSC thermograms of pristine SMPU and composites are presented in Fig. 9. It is observed that crystallization was seriously retarded in the presence of SiC and CNF, although the presence of organoclay and CB exerted small effects. In CNF and SiC composites, not only the total enthalpy of crystallization reduced significantly, the temperature intervals for the onset and end of crystallization remarkably shifted to lower temperatures.

We compared the crystallinity of composites of the present work with those reported in literature and found that CNF and SiC drastically reduced crystallinity in our systems. Paik et al. [63] reported only 7% reduction in soft segment crystallinity upon addition of 5 wt% MWNT to SMPU with PCL diol soft segments. Mondal and Hu [24] also observed only 7% decrease in soft segment crystallinity of an SMPU in the presence of 2.5 wt% MWNT. A potential reason for these relatively low crystallinity values of the composites in this work may be attributed to the sample preparation method. We mixed the nanoparticles in melt for 5 min, whereas other researchers [63,24] utilized solution mixing (2–12 h) and solvent evaporation (12–24 h) for longer periods of time. The solution mixing scheme and slow rates of solvent evaporation with time scales on the order of several hours may have provided longer time and allowed polymer chains to pack and crystallize in less viscous environment, even in the presence of fillers. Our data also suggest that the filler size, geometry, and the number of particles per unit volume might have played crucial roles in determining the crystallinity. For example, CB particles did not affect the crystallinity significantly, as expected. CB particles used were micrometer size fillers, with characteristic aggregate size of 0.4–1.0 μm [64] and were larger than the length scale of typical crystalline lamellae of about 10 nm [65]. Hence, it is unlikely that CB particles interfered with crystallization of soft segments. The filler geometry appears to be another crucial parameter when we compared organoclay/SMPU and CNF/SMPU composites. It was noted that in these composites crystallinity were different, although volumetric loading of filler, e.g., 2 vol% of organoclay vs. 3 vol% of CNF, and length scale for filler particles were similar. Therefore, the differences in crystallinity may be attributed to the filler geometry. The shapes of filler particles were different, e.g., thin platelets of clay were much more regular (Fig. 2) compared to irregular forms of CNF (Fig. 3). The presence of CNF with distorted shapes may prevent chain packing and ordering. On the other hand, it was observed in Figs. 7 and 8 that SiC particles also disturbed crystallization, even though the particle shape was fairly regular, almost spherical. We believe that a large decrease in crystallinity of soft segments in SiC/SMPU composite is related to the number of particles per unit volume, which was large in this case as revealed by the microscopic images in Fig. 4 showing a large number of well dispersed, almost spherical particles with relatively small diameters. It is thought that in SiC composites, chain packing might have been seriously hindered by the large number of well dispersed nanoscale SiC particles.

In view of the above-mentioned reasoning on crystallization of PCL diol soft segments in the presence of fillers, another series of composites were prepared separately in order to obtain further

Table 3
Soft segment melting temperatures of composites

Filler	Filler loading (wt%)							
	0		1		3		5	
	Melting point (°C)		Melting point (°C)		Melting point (°C)		Melting point (°C)	
	First scan	Second scan	First scan	Second scan	First scan	Second scan	First scan	Second scan
Organoclay	51	42	51	41	51	41	50	41
CB	51	42	50	39	51	40	54	46
CNF	51	42	48	37	47	36	46	33
SiC	51	42	48	36	46	34	45	33

The melting point is taken as the temperature that corresponds to the peak of the melting trace determined with DSC.

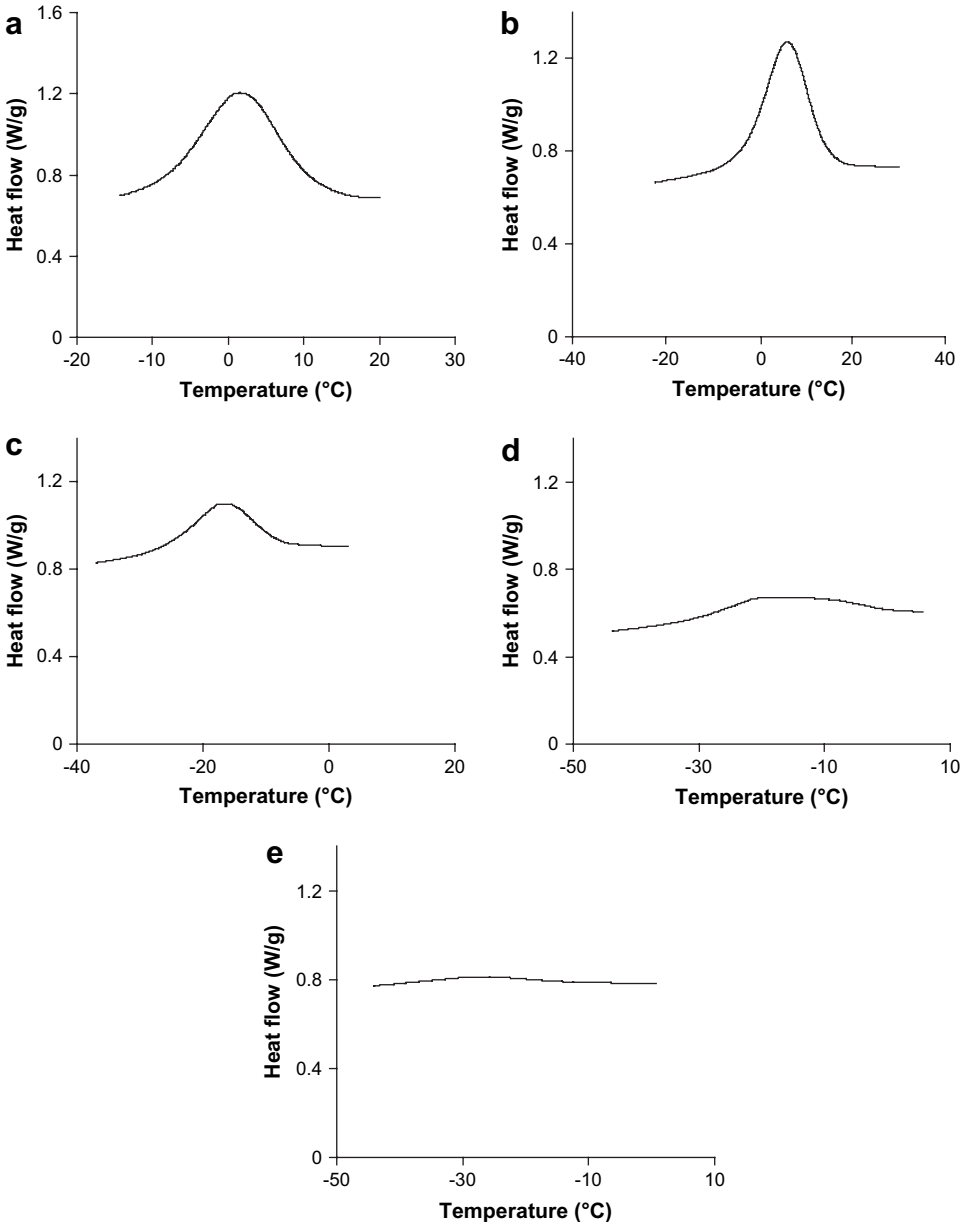

Fig. 9. Representative crystallization traces of pristine SMPU and its composites during cooling. Cooling rate is 20 °C/min. (a) Pristine SMPU; (b) CB/SMPU; (c) organoclay/SMPU; (d) CNF/SMPU; (e) SiC/SMPU.

understanding. In this second set of composites, neat PCL diol was used as the matrix material and the major aim was to compare the effects of fillers on crystallization of two different matrix materials of neat PCL diol and SMPU with PCL diol soft segments. The composites were prepared by mixing the fillers with neat PCL diol in Brabender internal mixer at 100 rpm for 5 min at 60 °C. The filler loading in these composites was adjusted to a level so as to give a similar weight ratio of filler and PCL diol as in SMPU composites. One may argue, however, about this weight ratio of filler in SMPU composites. The maximum filler loading in PCL diol segments of SMPU composites should have been 5 wt% (corresponding to 5 wt% filler loading), if an even distribution of fillers between hard domains and soft matrix of SMPU was assumed. On the other hand, the filler loading would be about 7 wt%, if the filler particles were considered to be located only in PCL diol soft segments. In view of this, we prepared PCL diol composites with up to 10 wt% filler content. The crystallinity data of these composites with 10 wt% filler particles, obtained during first and second scans, are summarized in Table 2. It is seen that there is only a small decrease in crystallinity of PCL diol upon addition of filler. Recall that the similar amounts of fillers also marginally reduced the crystallinity of PCL as reported by other investigators [66–71]. This observation, especially the data for CNF and SiC are in stark contrast to what was observed in Figs. 7 and 8 for the SMPU composites. One basic difference between SMPU composites and PCL diol composites is in the crystallization rates. PCL diol itself is a fast crystallizing polymer [72], whereas SMPU synthesized from PCL diol is a slow crystallizing one [73]. It appears that this difference in crystallization rates of matrix polymers may have played a decisive role in determining the crystallinity of composites.

In addition to the effects of fillers on soft segment crystallinity, we also analyzed the effects of fillers on hydrogen bonding using Fourier-transform infrared spectroscopy. In polyurethanes based on PCL diol, it is difficult to determine the degree of phase separation

from the data on hydrogen bonding. The carbonyl groups are present on both the soft and the hard segments, respectively, in the form of

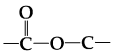

and

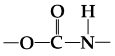

groups. Thus, we considered only the extent of hydrogen bonding formed by carbonyl groups using the area under the peaks of bonded (1700 cm^{-1}) and free carbonyl absorptions (1730 cm^{-1}). We observed that the ratio of area under the peak of hydrogen bonded C═O to that of free C═O was a constant (~0.4) for all composites and the neat SMPU. Note that a recent study reported significant changes in IR spectrum and phase separation in PU filled with zinc oxide [74]; it should be noted that filler–isocyanate reaction was allowed at the time of polymerization.

3.4. Shape memory properties

The shape memory properties, namely shape fixity (SF), shape recovery ratio (RR), and recovery stress, of the composites are discussed in this section. The data presented in Table 4 show that SF of pristine SMPU and all composites increase with stretching ratio from 30% to 100%. The SF of an SMP material is dictated by two main factors. First one is the amount of '*unlocked*' oriented chains and the chain segments. If an affine deformation is considered, all chains experience the same level of deformation in the stretching step (stage A, Fig. 1). The orientation of these stretched chains is preserved by crystallization of the soft segment in the cooling stage (stage B, Fig. 1). Nevertheless, a certain fraction of the chains and chain segments preserve mobility, e.g., the chain segments which do not crystallize. These '*unlocked*' chains generate an instantaneous retractive force upon removal of the tensile load due to entropic elasticity. However, this retractive force alone cannot lead to instantaneous recovery of the shape as the fraction of mobile chains is usually low. The second crucial factor is the modulus of the material at room temperature. The instantaneous retractive force can cause only limited instantaneous recovery strain if the room temperature modulus is high. On the other hand, a low value of SF and more rapid recovery occur if the value of modulus is low.

Our data indicate that organoclay did not exert significant effect on SF of SMPU (Table 4), while CNF and SiC particles reduced the value of SF. It is also noted from Table 4 that the addition of CB particles did not exert much effect on the shape memory properties at lower loadings. However, between 3 wt% and 5 wt% CB loading, the filler particles formed continuous networks as revealed from the measurement of electrical conductivity [75]. It was found that the composite became electrically conductive beyond a CB loading of about 3 wt%. These particle networks destroyed all the shape memory properties of the composites. For example, beyond the critical loading level of about 3 wt%, the material did not show any elastomeric properties at 60 °C and hence could not be stretched properly – the samples broke beyond 10% strain.

Table 4
Shape fixity (SF) of composites

Filler	Filler loading (wt%)											
	0			1			3			5		
	Strain (%)			Strain (%)			Strain (%)			Strain (%)		
	30	60	100	30	60	100	30	60	100	30	60	100
	SF (%)			SF (%)			SF (%)			SF (%)		
Organoclay	62	74	93	62	88	100	72	79	100	67	82	96
CB	62	74	93	63	79	95	61	79	78	N.A.	N.A.	N.A.
CNF	62	74	93	29	41	46	24	31	38	19	21	29
SiC	62	74	93	48	57	77	32	67	64	29	38	46

The composite of 5 wt% CB failed at about 10% elongation and corresponding data were not available.

Table 5
Shape recovery ratio (RR) of composites

Filler	Filler loading (wt%)											
	0			1			3			5		
	Strain (%)			Strain (%)			Strain (%)			Strain (%)		
	+30	60	100	30	60	100	30	60	100	30	60	100
	RR (%)			RR (%)			RR (%)			RR (%)		
Organoclay	72	83	80	66	75	74	63	76	74	69	75	73
CB	72	83	80	69	81	79	78	78	79	N.A.	N.A.	N.A.
CNF	72	83	80	66	80	83	60	59	76	50	50	60
SiC	72	83	80	83	82	82	63	85	80	50	69	75

The composite of 5 wt% CB did not show shape recovery.

The values of shape recovery ratio (RR) of composites are presented in Table 5 and they follow similar trends as SF. The composites of CNF and SiC show gradual decrease in RR with the addition of filler, while the composite of organoclay shows insensitivity to the filler content. It is also noted in Table 5 that CB had weak influence on RR at lower filler loadings, while at 5 wt% CB loading the composite lost shape memory properties.

The values of recovery stress are presented in Table 6. As it is known in the context of heat shrinkable polymers [76,77], the recovery stress vs. temperature plot shows a bell-shaped curve as the material is heated gradually starting from the room temperature. The shape is dictated by the number of chains undergoing recovery upon heating. The number of recovering chains increases with an increase in temperature, reaches a maximum, and then starts declining at temperatures higher than the temperature at which the particle was deformed. Our data in Table 6 show that the presence of CNF and SiC particles drastically decreased the value of recovery stress, while the presence of organoclay increased the recovery stress especially at higher stretching ratios. It is noted that the inclusion of CB provided marginal increase of recovery stress only at 3 wt% loading. The composite of 5 wt% CB did not show shape memory behavior.

A few words are in order on the magnitude of recovery stress of pristine SMPU and its composites. The values of recovery stress determined in this work are typical – about 1–3 MPa with 100% strain, obtained from compression and injection molded or solution cast SMPU systems [3]. On the other hand, considerably higher recovery stress values of about 150 MPa were recently reported for SMP nanocomposite fibers recovering from a strain of about 800% [78]. It is apparent that these two magnitudes of recovery stress are very different owing to the differences in the stretching ratio and the sample preparation method. In a polymer network, the recovery stress is dictated by the stretching ratio, cross-link density, and the presence of reinforcing fillers [79]. Besides, the order and

Table 6
Recovery stress of composites

Filler	Filler loading (wt%)											
	0			1			3			5		
	Strain (%)			Strain (%)			Strain (%)			Strain (%)		
	30	60	100	30	60	100	30	60	100	30	60	100
	Stress (MPa)			Stress (MPa)			Stress (MPa)			Stress (MPa)		
Organoclay	0.82	2.20	2.44	0.96	2.92	3.20	0.82	2.42	3.04	0.84	2.77	3.12
CB	0.82	2.20	2.44	0.82	1.98	2.32	1.56	1.92	2.65	N.A.	N.A.	N.A.
CNF	0.82	2.20	2.44	0.84	1.45	1.76	0.04	0.64	1.69	0.00	0.17	0.59
SiC	0.82	2.20	2.44	0.80	1.10	1.73	0.56	1.01	1.80	0.07	0.36	1.32

orientation of physical cross-link sites also influence the recovery stress in certain non-Gaussian networks [80]. Hard domains in polyurethanes [5] and crystalline *fixed phases* in certain shape memory polymers [78] are examples of cross-link sites. Processing conditions, such as shear rate, shear stress, and cooling rate, experienced by the polymer are known to exert influence on the order and orientation of these physical cross-link sites which in turn can affect the magnitude of recovery stress.

The data in Tables 4–6 and Fig. 7 also indicate that there is a direct correlation between the degree of crystallinity of soft segments and shape memory properties. It was seen earlier that the soft segment crystallinity and shape memory performance decreased in the presence of CNF and SiC. Our results suggest that owing to decreased crystallinity, chain orientation was not preserved effectively after the tensile load was removed. First, this inadequate crystallinity created more '*unlocked*' chains and hence promoted instantaneous recovery. Second, it also decreased the room temperature modulus and thus decreased the resistance to instantaneous recovery. Consequently, SF ratios were significantly lower in CNF and SiC composites, as seen in Table 4. Due to the fact that organoclay and CB exerted only a slight impact on soft segment crystallinity, the SF values were not reduced in organoclay and CB composites, except in the composite with 5 wt% CB which lost all shape memory properties. Lower levels of crystallinity would further decrease RR and recovery stress, due to higher fractions of '*unlocked*' chains and chain segments. In view of the data presented in Tables 4–6, organoclay is the only promising filler for the SMPU considered in this paper. It was found that organoclay addition did not alter the SF and RR of pristine SMPU and instead augmented the recovery stress. This increase in recovery stress is thought to be related to mechanical reinforcement effects of the filler, especially in view of excellent exfoliation (Fig. 2). However, it should be also mentioned that the level of increase in recovery stress upon organoclay addition had been lower than our expectation, as will be addressed later.

In next section we present results on tensile properties of the composites at 60 °C in order to gain more insight on the modulus vs. recovery stress relationship and the extent of mechanical reinforcement due to the presence of fillers. Note that all soft segment crystals melted at 60 °C and the tensile stress observed during the stretching might be a measure of the recovery stress in an ideal SMP. We also analyze the relationship between tensile modulus and recovery stress in organoclay/SMPU nanocomposite. Analysis of this relation is not fruitful for composites of other fillers due to inferior shape memory properties.

3.5. Tensile properties of composites at 60 °C and hysteresis behavior

Fig. 10 shows typical tensile stress–strain plots of pristine SMPU at room temperature and at 60 °C. The stress–strain plot determined at room temperature (25 °C) closely resembles that of usual semi-crystalline polymers with a clearly distinguishable yielding behavior. Note, however, that the SMPU included in this study acted like a typical elastomer with relatively lower tensile modulus at 60 °C, as all the crystals melted at this temperature. The tensile modulus determined at room temperature from tensile stress–strain plots of composites (Table 7) indicated that the modulus increased in the presence of organoclay and CB while it greatly decreased in the presence of CNF and SiC. As seen before, this reduction was due to the decreased soft segment crystallinity.

Fig. 11 shows typical stress–strain plots determined at 60 °C for all composites. These plots indicate the effects of different fillers on the stored stress during stretching of the composites. The tensile moduli of composites determined from these stress–strain plots are presented in Table 7. Both CNF (Fig. 11a) and SiC (Fig. 11b) exerted

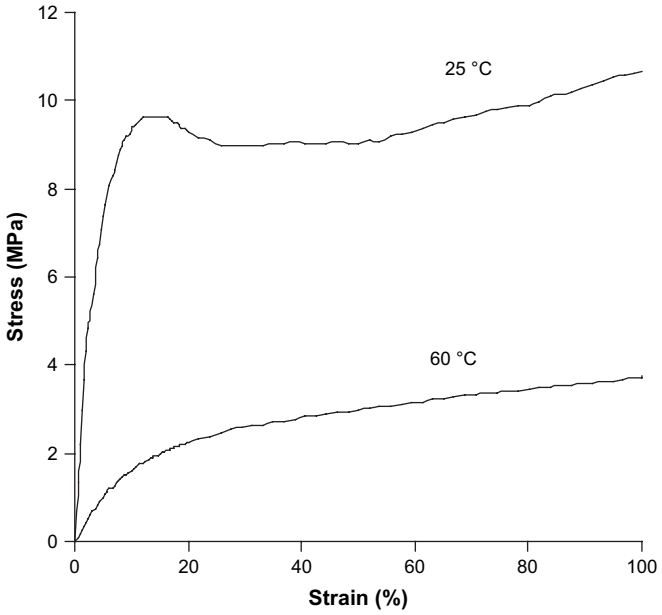

Fig. 10. Typical stress vs. strain plot of pristine SMPU at room temperature (25 °C) and at 60 °C. Stretching rate was 50 mm/min.

little impact on tensile properties of SMPU, especially on tensile moduli at 60 °C. Table 7 reveals that incorporation of CNF caused almost no increase in the tensile moduli. The same behavior was observed for CNF/PMMA nanocomposites [40]. Other investigators reported similar results [81–85]. These observations are in stark contrast to the predictions of composite models, in light of the remarkably higher modulus of CNF (~600 GPa), as addressed previously. Previous work [40] suggests that at low filler loadings, the aspect ratio also plays a minor role in dictating the values of tensile modulus of nanocomposites. In addition, it was also shown that high shear melt processing, the same processing scheme adopted in this work, decreased the number of fiber bundles significantly, hence incomplete infiltration was probably not responsible for poor tensile modulus in composites of CNF. Tibbetts and McHugh [83] established the importance of CNF surface characteristics on mechanical properties. The scarcity of polar functional groups on the surface of CNF used in this work [41] suggests that the lack of proper interfacial adhesion was responsible for insignificant improvement in tensile properties. However, further analysis of this issue was beyond the scope of this study.

Tensile properties of SiC/SMPU (Fig. 11b and Table 7) composite showed a behavior similar to that of CNF/SMPU composite. SiC addition decreased the modulus at room temperature as a result of the decrease in crystallinity. However, it augmented the values of modulus at 60 °C, although the level of reinforcement is relatively small due to low aspect ratio (~1) of the spherical particles. Although previous studies reported deterioration of mechanical properties beyond a SiC loading of about 1.5 wt% in SiC/epoxy and

Table 7
Tensile moduli of composites at room temperature and at 60 °C

Filler	Filler loading (wt%)							
	0		1		3		5	
	Modulus (MPa)		Modulus (MPa)		Modulus (MPa)		Modulus (MPa)	
	25 °C	60 °C	25 °C	60 °C	25 °C	60 °C	25 °C	60 °C
Organoclay	170.0	24.3	176.0	30.2	256.0	39.9	272.0	49.8
CB	170.0	24.3	186.0	28.5	232.0	28.9	469.0	47.6
CNF	170.0	24.3	81.0	27.6	38.0	22.9	27.0	23.9
SiC	170.0	24.3	101.0	24.7	54.0	30.9	36.0	26.5

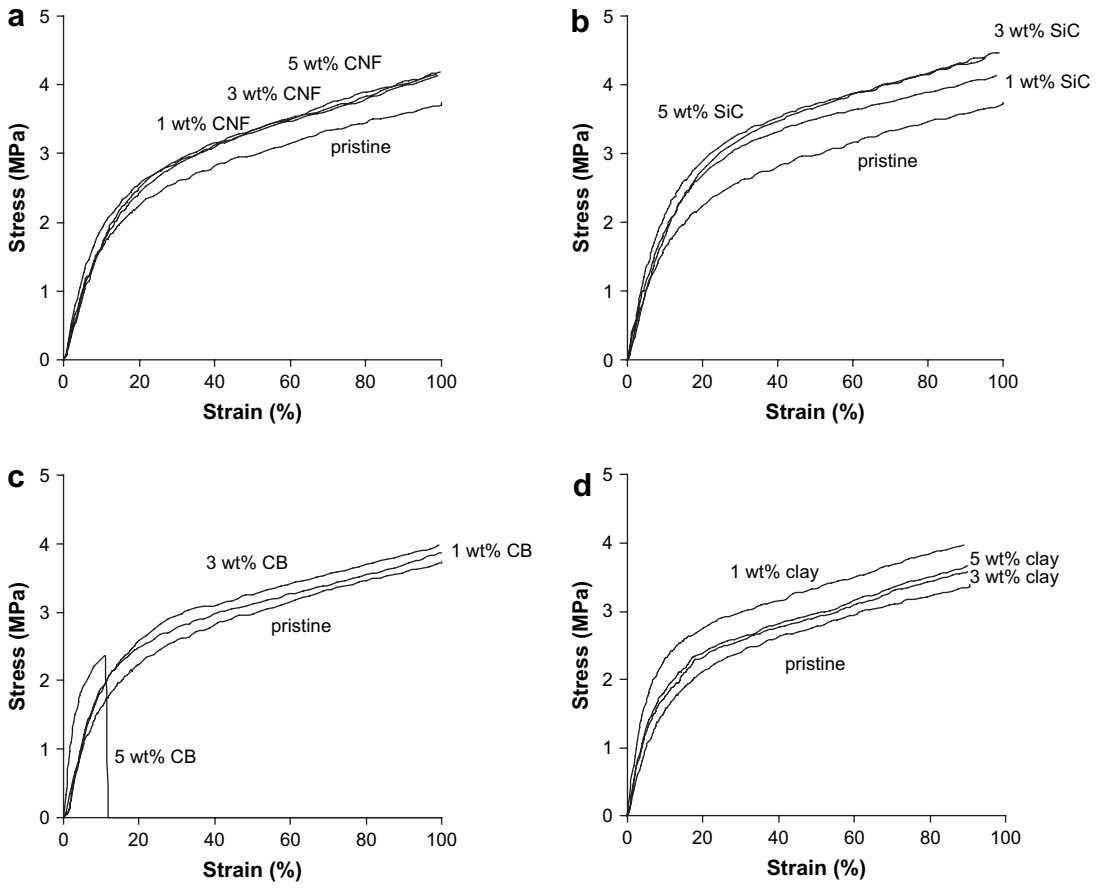

Fig. 11. Typical stress–strain plots of composites at 60 °C. Stretching rate was 50 mm/min. (a) CNF/SMPU; (b) SiC/SMPU; (c) CB/SMPU; (d) organoclay/SMPU.

SiC/PU foam composites [86,87], our data do not indicate such a behavior. The presence of CB up to 3 wt% loading also failed to cause any significant reinforcement (Fig. 11c). Beyond this loading, there is a remarkable augmentation in modulus; however, the composite became brittle. CB addition slightly increased the modulus up to a loading of about 3 wt% (Table 7), both at room temperature and at 60 °C. Note that the modulus at 25 °C increased from 232 MPa for 3 wt% CB to 469 MPa for 5 wt% CB. These data suggest that continuous networks of filler were formed at these filler loading which were responsible for this drastic increase in tensile moduli.

Organoclay/SMPU nanocomposite (Fig. 11d) showed a different behavior than other systems. The value of stretching stress was the highest for composites with 1 wt% organoclay. The value of stretching stress of composites with 3 wt% and 5 wt% organoclay fell between the value of nanocomposite of 1 wt% organoclay and that of the pristine SMPU. A similar observation was reported previously for organoclay/SMPU nanocomposite [26], and the increased stress relaxation in the presence of large amounts of organoclay was observed to be the primary reason behind reduced level of stress in composites of 3 wt% and 5 wt% organoclay. On the other hand, the tensile moduli data at 60 °C (Table 7) indicate the reinforcement effect of organoclay on tensile moduli and hence a gradual augmentation of tensile modulus upon addition of organoclay. However, we fail to observe a direct proportionality between the tensile modulus and highest stretching stress. For example, composite of 1 wt% clay content gave highest stretching stress, although highest tensile modulus was obtained with 5 wt% clay. Likewise, we also fail to observe any direct relationship between tensile moduli and recovery stress. For example, the tensile modulus at room temperature increased by 60% and that at 60 °C by 100% in the presence of 5 wt% organoclay. At the same time, recovery stress increased by only 30% with the addition of 5 wt% organoclay. We propose the following potential reasons for the relatively lower increase of recovery stress in the presence of organoclay. First, organoclay exerted a small negative effect on the soft segment crystallinity. This is the first potential reason for a lower recovery stress. Second, although organoclay addition did not change the level of hydrogen bonding in our system, DSC data indicated that it might have interfered with the order of the hard domains [26]. The DSC traces showed a clear decrease in heat of fusion which corresponds to melting of the hard domains, at about 220 °C. Note also that the organoclay particles had more opportunity to interact with the hard segments as a consequence of our synthesis scheme [30–32]. It is conceivable that disordered hard domains may lead to higher relaxation rates of oriented chains and chain segments of SMPU which consequently would result in lower recovery stresses. Another possibility is the extent of organoclay dispersion. As suggested previously [88,89], better exfoliation leads to lower relaxation rate in PU/organoclay nanocomposites. We obtained best organoclay exfoliation in the case of 1 wt% organoclay loading. Hence, it is also a possibility that further organoclay addition caused faster relaxation owing to less perfect dispersion.

We observed that recovery stress and tensile stretching stress at 60 °C of the composites are decoupled, especially for CNF/SMPU and SiC/SMPU composites, as evident from the data presented in Table 6 and Fig. 11. As seen above, the lack of adequate soft segment crystallinity in the presence of fillers, and resulting large number of '*unlocked*' chains and chain segments were the principal reasons for this decoupling.

The composites were also subjected to repeated shape memory testing cycles in order to elaborate the hysteresis behavior of SMPU

Table 8
Tensile moduli of composites at 60 °C determined in cyclic loading

Filler	Filler loading (wt%)							
	0		1		3		5	
	Modulus (MPa)		Modulus (MPa)		Modulus (MPa)		Modulus (MPa)	
	Cycle I	Cycle II	Cycle I	Cycle II	Cycle I	Cycle II	Cycle I	Cycle II
Organoclay	24.3	13.1	30.2	13.5	39.9	23.6	49.8	26.9
CB	24.3	13.1	28.5	14.9	28.9	12.4	47.6	45.6
CNF	24.3	13.1	27.6	18.9	22.9	17.5	23.9	12.3
SiC	24.3	13.1	24.7	13.9	30.9	18.8	26.5	14.4

composites. We report here the tensile modulus values at 60 °C, in order to eliminate any potential artifact originating from the filler–crystallinity interactions. A set of samples were stretched only once (designated as Cycle I) at 60 °C and another set of samples were stretched again at this temperature for the second time after initial stretching and following relaxation (designated as Cycle II). Corresponding results are presented in Table 8. The cyclic loading data on tensile moduli at 60 °C indicate that the fillers did not exert any effect on hysteresis of shape memory properties of the nanocomposites. These data suggest that the nanofillers did not interfere with the deformation and orientation of polyurethane segments, and the observed hysteresis originated solely from the matrix polymer. Earlier work indicates that hysteresis in polyurethanes upon cyclic loading originates from the plastic deformation of hard domains and it depends on the strain experienced by the polymer [90–93].

4. Conclusions

The study showed that a strong correlation exists between soft segment crystallinity and shape memory performance. Although nanoparticles were used with the expectation that SMPU performance would be significantly improved, mixed results were produced due to interference of nanoparticles with the soft segment crystallinity. Our data showed that the filler particles interfered with crystallization due to comparable sizes of the filler and the typical crystal lamellae. The soft segment crystallinity was drastically reduced in the presence of CNF and SiC. The materials with CB loading higher than 3 wt% also failed to show useful shape memory properties due to brittleness. SM performance of composites of CNF, SiC, and CB was inferior to that of pristine SMPU and organoclay/SMPU composites. Nevertheless, in all composites, higher shape memory properties were observed at higher stretching ratios, as a consequence of strain induced crystallization of the soft segment. It was noted that CNF and SiC did not significantly augment tensile modulus and stretching stress, while CB remarkably increased tensile modulus at about 5 wt% filler content, although the resulting composite was extremely brittle and all shape memory properties were lost. In organoclay/SMPU nanocomposites, the highest stretching stress and recovery stress values were observed with 1 wt% filler content, although tensile moduli gradually increased with organoclay addition. Cyclic tensile testing data revealed that fillers did not exert any effect on hysteresis characteristics of SMPU.

Acknowledgments

Partial financial support for this work was provided by National Science Foundation in the form of CAREER Award (DMI-0134106) to SCJ. Authors gratefully acknowledge Dr. Rex Ramsier and Justin Walker for their help with XPS data.

References

[1] Hayashi S, Kondo S, Kapadia P, Ushioda E. Plast Eng 1995;51:29–31.
[2] Gunes IS, Jana SC. J Nanosci Nanotechnol 2008;8:1616–37.
[3] Lendlein A, Kelch S. Angew Chem Int Ed 2002;41:2034–57.
[4] Beloshenko VA, Varyukhin VN, Voznyak YuV. Russ Chem Rev 2005;74:265–83.
[5] Liu C, Qin H, Mather PT. J Mater Chem 2007;17:1543–58.
[6] Kim BK, Lee SY, Xu M. Polymer 1996;37:5781–93.
[7] Kamieneski EL, Mandelbaum S, Vemuri P, Weiss RA. Proc SPE ANTEC 2007: 2714–7.
[8] Jimenez GA, Jana SC. Proc SPE ANTEC 2007:18–22.
[9] Mohr R, Kratz K, Weigel T, Lucka-Gabor M, Moneke M, Lendlein A. Proc Natl Acad Sci USA 2006;103:3540–5.
[10] Maitland DJ, Metzger MF, Schumann D, Lee A, Wilson TS. Lasers Surg Med 2002;30:1–11.
[11] Treloar LRG. The physics of rubber elasticity. 2nd ed. Oxford: Clarendon Press; 1958 [chapter 4].
[12] Mark JE. J Chem Educ 1981;58:898–903.
[13] Wei ZG, Sandstrom R, Miyazaki S. J Mater Sci 1998;33:3743–62.
[14] U.S. Patent 3,284,275, 1966.
[15] Hayashi S. Int Prog Urethanes 1993;6:90–115.
[16] Poilane C, Delobelle P, Lexcellent C, Hayashi S, Tobushi H. Thin Solid Films 2000;379:156–65.
[17] Tobushi H, Matsui R, Hayashi S, Shimada D. Smart Mater Struct 2004;13: 881–7.
[18] Liang C, Rogers CA, Malafeew E. J Intell Mater Syst Struct 1997;8:380–6.
[19] Ohki T, Ni Q-Q, Ohsako N, Iwamoto M. Composites Part A 2004;35:1065–73.
[20] Li F, Qi L, Yang J, Xu M, Luo X, Ma D. J Appl Polym Sci 2000;75:68–77.
[21] Yang B, Huang WM, Li C, Chor JH. Eur Polym J 2005;41:1123–8.
[22] Gall K, Dunn ML, Liu Y, Finch D, Lake M, Munshi NA. Acta Mater 2002;50: 5115–26.
[23] Gall K, Dunn ML, Liu Y, Stefanic G, Balzar D. Appl Phys Lett 2004;85:290–2.
[24] Mondal S, Hu JL. Iran Polym J 2006;15:135–42.
[25] Koerner H, Price G, Pearce NA, Alexander M, Vaia RA. Nat Mater 2004;3: 115–20.
[26] Cao F, Jana SC. Polymer 2007;48:3790–800.
[27] Li F, Hou J, Zhu W, Zhang X, Xu M, Luo X, et al. J Appl Polym Sci 1996;62:631–8.
[28] Kim HJ, Worley II DC, Benson RS. Polymer 1997;38:2609–14.
[29] Verhelst WF, Wolthuis KG, Voet A, Ehrburger P, Donnet JB. Rubber Chem Technol 1977;50:735–46.
[30] Pattanayak A, Jana SC. Polymer 2005;46:3275–88.
[31] Pattanayak A, Jana SC. Polymer 2005;46:3394–406.
[32] Pattanayak A, Jana SC. Polymer 2005;46:5183–93.
[33] Chen TK, Tien YI, Wei KH. Polymer 2000;41:1345–53.
[34] Tien Yi, Wei KH. Macromolecules 2001;34:9045–52.
[35] Chavarria F, Paul DR. Polymer 2006;47:7760–73.
[36] Agari Y, Uno T. J Appl Polym Sci 1985;30:2225–35.
[37] Lee G-W, Park M, Kim J, Lee JI, Yoon HG. Composites Part A 2006;37: 727–34.
[38] Xu Y, Ray G, Abdel-Magid B. Composites Part A 2006;37:114–21.
[39] Yao KJ, Song M, Hourston DJ, Luo DZ. Polymer 2002;43:1017–20.
[40] Jimenez GA, Jana SC. Composites Part A 2007;38:983–93.
[41] Jimenez GA, Jana SC. Carbon 2007;45:2079–91.
[42] Yong V, Hahn HT. Nanotechnology 2004;15:1338–43.
[43] Rodgers RM, Mahfuz H, Rangari VK, Chisholm N, Jeelani S. Macromol Mater Eng 2005;290:423–9.
[44] Onneby C, Pantano CG. J Vac Sci Technol A 1997;15:1597–602.
[45] Hijikata Y, Taguchi H, Yoshikawa M, Yoshida S. Appl Surf Sci 2001;184:161–6.
[46] Hornetz B, Michel H-J, Halbritter J. J Vac Sci Technol A 1995;13:767–71.
[47] Omastova M, Boukerma K, Chehimi MM, Trchova M. Mater Res Bull 2005;40: 749–65.
[48] Okuyama M, Garvery GJ, Ring TA, Haggerty JS. J Am Ceram Soc 1989;72: 1918–24.
[49] Brooks CS, DeCrescente MA, Scola DA. J Colloid Interface Sci 1968;27:772–88.
[50] Wittberg TN, Wang PS, Hsu SM. Surf Interface Anal 2003;35:773–8.
[51] Bermudez VM. J Appl Phys 1989;66:6084–92.
[52] Crescenzi V, Manzini G, Calzolari G, Borri C. Eur Polym J 1972;8:449–63.
[53] Ou-Yang W-C, Li L-J, Chen H-L, Hwang JC. Polym J 1997;29:889–93.
[54] Ping P, Wang W, Chen X, Jing X. Biomacromolecules 2005;6:587–92.
[55] Morbitzer L, Hespe H. J Appl Polym Sci 1972;16:2697–708.
[56] Koerner H, Liu W, Alexander M, Mirau P, Dowty H, Vaia RA. Polymer 2005;46: 4405–20.
[57] Konyukhova EV, Neverov VM, Chvalun SN, Godovsky Yu K. Polym Sci Ser A 2004;46:61–74.
[58] Curgul S, Yilgor I, Yilgor E, Erman B, Cakmak M. Macromolecules 2004;37: 8676–85.
[59] Fornes TD, Paul DR. Polymer 2003;44:4993–5013.
[60] Lemieux S, Elomari S, Nemes JA, Skibo MD. J Mater Sci 1998;33:4381–7.
[61] Dharaiya DP, Jana SC, Lyuksyutov SF. Polym Eng Sci 2006;46:19–28.
[62] Mandelkern L. The crystalline state. In: Mark JE, Eisenberg A, Graessley WW, Madnelkern L, Samulski ET, Koenig JL, Wignall GD, editors. Physical properties of polymers. 2nd ed. Washington, D.C.: American Chemical Society; 1993. p. 147–51.
[63] Paik IH, Goo PS, Jung YC, Cho JW. Smart Mater Struct 2006;15:1476–82.
[64] Medalia AI. In: Sichel EK, editor. Carbon black-polymer composites: the physics of electrically conducting composites. New York: Marcel Dekker Inc.; 1982. p. 1–49.
[65] Donth E-J. Relaxation and thermodynamics in polymers: glass transition. Berlin: Akademie Verlag; 1992. p. 25–27.
[66] Jimenez G, Ogata N, Kawai H, Ogihara T. J Appl Polym Sci 1997;64:2211–20.

[67] Lepoittevin B, Devalckenaere M, Pantoustier N, Alexandre M, Kubies D, Calberg C, et al. Polymer 2002;43:4017–23.
[68] Kiersnowski A, Piglowski J. Eur Polym J 2004;40:1199–207.
[69] Di Maio E, Iannace S, Sorrentino L, Nicolais L. Polymer 2004;45:8893–900.
[70] Homminga D, Goderis B, Dolbnya I, Groeninckx G. Polymer 2006;47:1620–9.
[71] Wu T-M, Chen E-C. Polym Eng Sci 2006;46:1309–17.
[72] Phillips PJ, Rensch GJ, Taylor KD. J Polym Sci Part B Polym Phys 1987;25:1725–40.
[73] Ping P, Wang W, Chen X, Jing X. J Polym Sci Part B Polym Phys 2007;45:557–70.
[74] Zheng J, Ozisik R, Siegel RW. Polymer 2005;46:10873–82.
[75] Gunes IS, Cao F, Jimenez GA, Jana SC. Proc SPE ANTEC 2007:1362–6.
[76] Decandia F, Russo R, Vittoria V, Peterlin A. J Polym Sci Part B Polym Phys 1982;20:1175–92.
[77] Decandia F, Romano G, Vittoria V, Peterlin A. J Appl Polym Sci 1985;30:4159–73.
[78] Miaudet P, Derre A, Maugey M, Zakri C, Piccione PM, Inoubli R, et al. Science 2007;318:1294–6.
[79] Erman B, Mark JE. Structures and properties of rubberlike networks. New York: Oxford University Press; 1997 [chapter 2].
[80] Bonart R. Polymer 1979;20:1389–403.
[81] Carneiro OS, Covas JA, Bernardo CA, Caldeira G, Van Hattum FWJ, Ting J-M, et al. Compos Sci Technol 1998;58:401–7.
[82] Calderia G, Maia JM, Carneiro OS, Covas JA, Bernardo JA. Polym Compos 1998;19:147–51.
[83] Tibbetts GG, McHugh JJ. J Mater Res 1999;14:2871–80.
[84] Patton RD, Pittman Jr CU, Wang L, Hill JR. Composites Part A 1999;30:1081–91.
[85] Gao Y, He P, Lian J, Schulz MJ, Zhao J, Wang W, et al. J Appl Polym Sci 2007;103:3792–7.
[86] Chisholm N, Mahfuz H, Rangari VK, Ashfaq A, Jeelani S. Compos Struct 2005;67:115–24.
[87] Mahfuz H, Rangari VK, Islam MS, Jeelani S. Composites Part A 2004;35:453–60.
[88] Dai XH, Xu J, Guo XL, Lu YL, Shen DY, Zhao N, et al. Macromolecules 2004;37:5615–23.
[89] Xia HS, Shaw SJ, Song M. Polym Int 2005;54:1392–400.
[90] Estes GM, Seymour RW, Cooper SL. Macromolecules 1971;4:452–7.
[91] Seymour RW, Allegrezza Jr AE, Cooper SL. Macromolecules 1973;6:896–902.
[92] Allegrezza Jr AE, Seymour RW, Ng HN, Cooper SL. Polymer 1974;15:433–40.
[93] Seymour RW, Cooper SL. Rubber Chem Technol 1974;47:19–31.